

Behind Armor Debris computations with finite elements and meshless particles

Gordon R. Johnson and Robert A. Stryk
also

Stephen R. Beissel and Charles A. Gerlach

Army High-Performance Computing Research Center
Network Computing Services, Inc; Minneapolis, MN

22nd International Symposium on Ballistics
Vancouver, BC, Canada

November 14-18, 2005

Acknowledgement

This presentation was performed in connection with the Army High-Performance Computing Research Center Infrastructure Contract (DAAD19-03-D-0001) with the U.S. Army Research Laboratory.

The views and conclusions contained in this presentation are those of the authors and should not be interpreted as presenting the official policies or positions, either expressed or implied, of the U.S. Army Research Laboratory or the U. S. Government unless so designated by other authorized documents. Citation of manufacturer's or trade names does not constitute an official endorsement or approval of the use thereof.

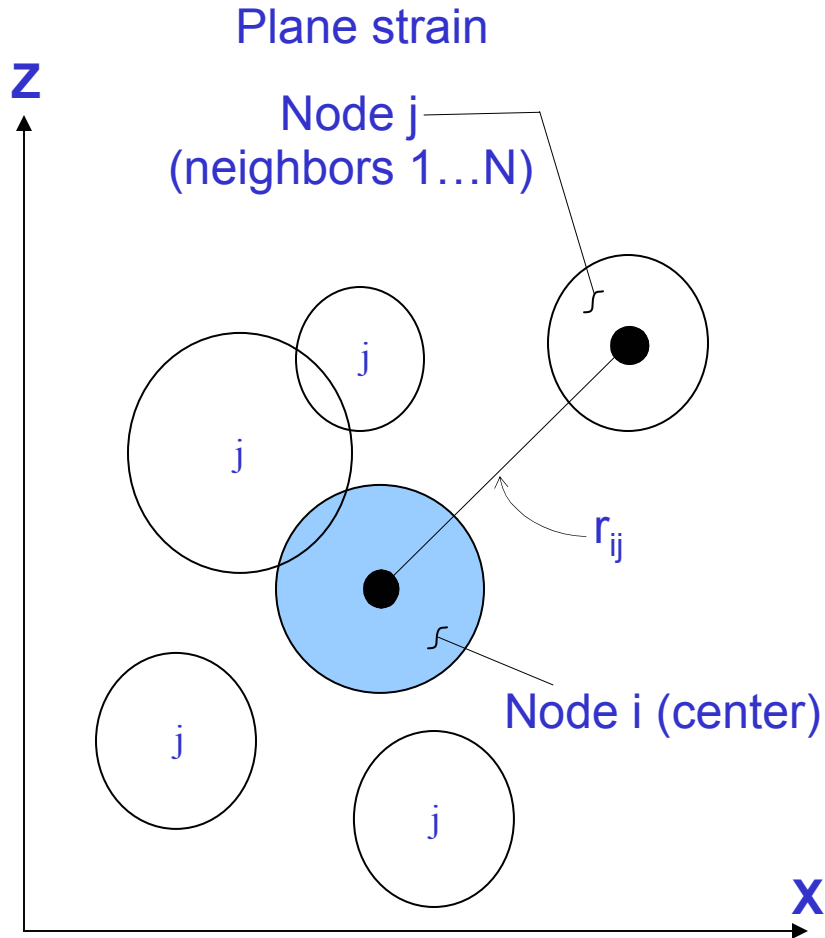
Outline

- Comments regarding Behind Armor Debris (BAD)
- Generalized Particle Algorithm (GPA)
- Conversion of finite elements to particles
- Description of computed fragments
- Computations of Behind Armor Debris
 - EPIC code
 - Ballistic velocities and hypervelocities
 - Computations compared to experiments
- Summary
- Movie (if time permits)

Comments regarding Behind Armor Debris

- Determination of BAD from testing is difficult
 - Requires fragment material, size, velocity, position
 - Another approach is to collect fragments in witness pack
- Determination of BAD from computations is difficult
 - Eulerian algorithms have trouble with large air gaps
 - Finite element algorithms have trouble with large distortions
 - Meshless particle algorithms may have trouble with accuracy
- Combination of finite elements and meshless particles is well suited for BAD computations

Generalized Particle Algorithm



Data from neighbors is required for gradients

strain rates

$$\dot{\epsilon}_{xx}^i = \sum_{j=1}^N \frac{-R_{ij} A_i A_j}{r_{ij}} \left[\alpha_x^i (v_x^j - v_x^i) l_x^{ij} \right]$$

forces

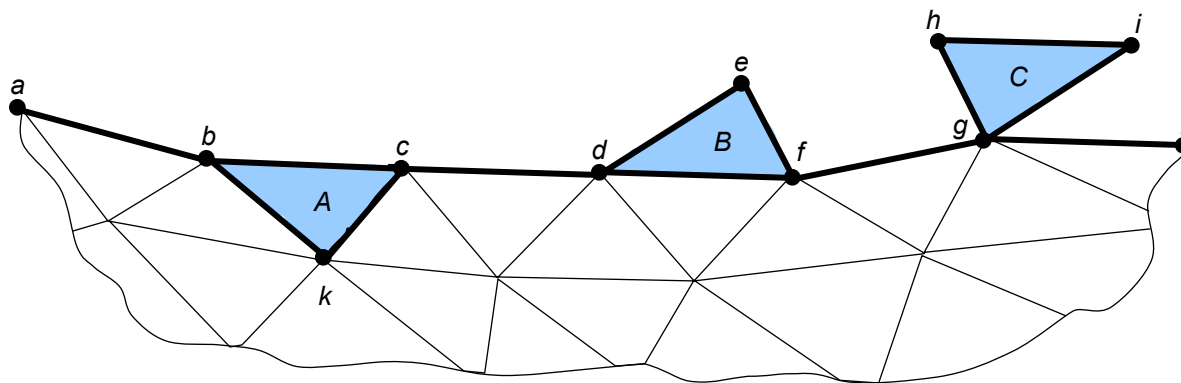
$$P_x^i = \sum_{j=1}^N \frac{-R_{ij} A_i A_j}{r_{ij}} \left[\alpha_x^i (\sigma_{xx}^i - Q_{ij}) l_x^{ij} + \alpha_z^i \sigma_{xz}^i l_z^{ij} \right]$$

where

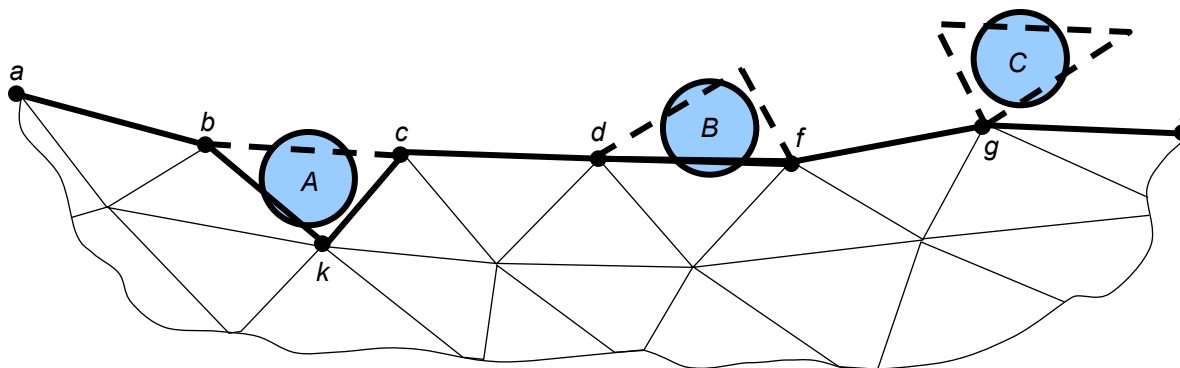
$$\alpha_x^i = \frac{1}{\sum_{j=1}^N R_{ij} A_j (l_x^{ij})^2}$$

Conversion of finite elements to particles

Interface nodes and elements before conversion



Interface after conversion of elements



Capabilities of Lagrangian conversion algorithm

- Penetration and perforation of target
- Failure and fragmentation of material
- Highly distorted flow and structural deformations
- Accurate contact and sliding between materials
- Travel through large air gaps
 - no numerical diffusion of geometry or materials
 - no element or particle representation of air gaps
- Interaction with subsequent target components

Conversion of finite elements to particles

Ballistic velocities

$V = 2000 \text{ m/s}$

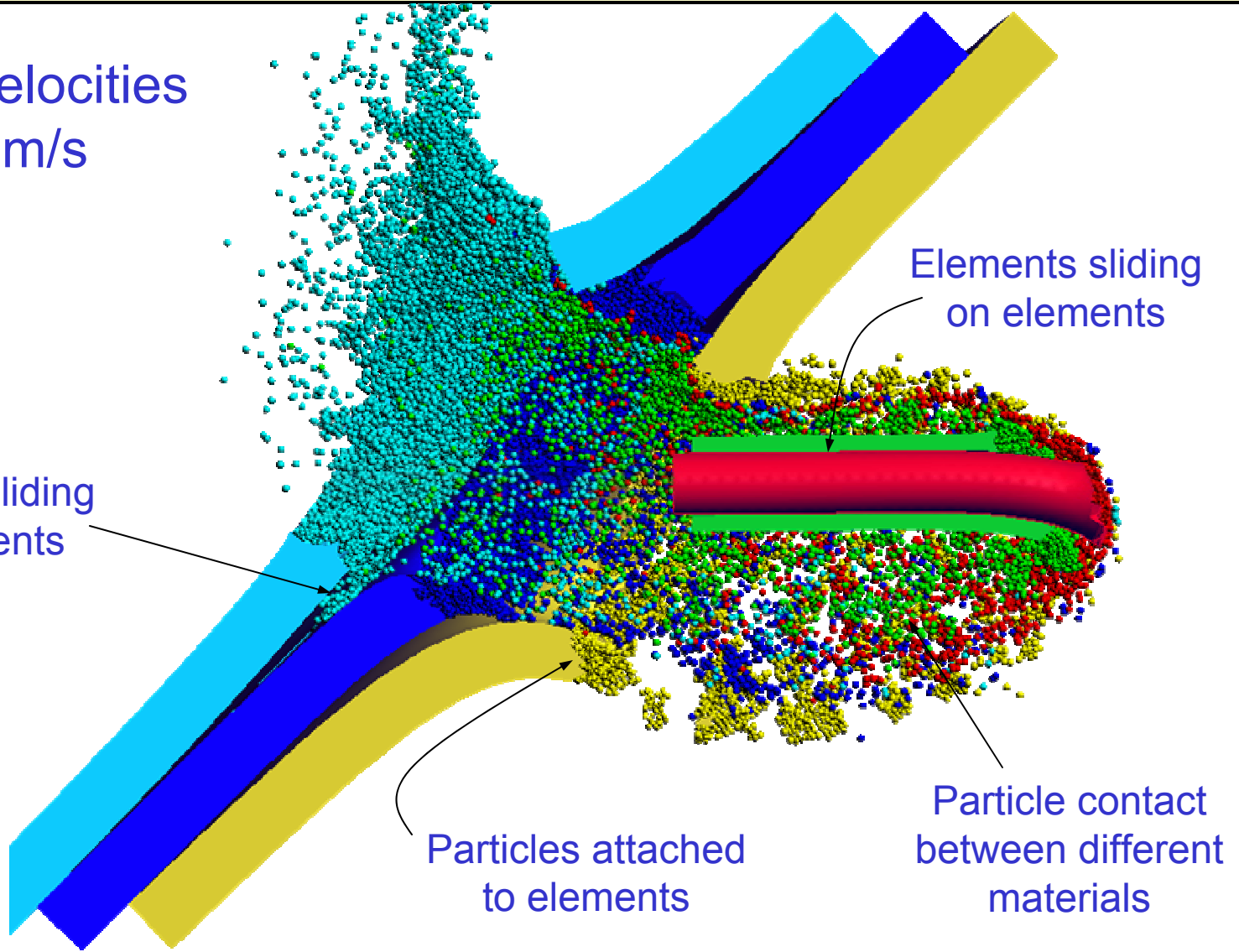
$t = 100 \mu\text{s}$

Particles sliding
on elements

Elements sliding
on elements

Particles attached
to elements

Particle contact
between different
materials

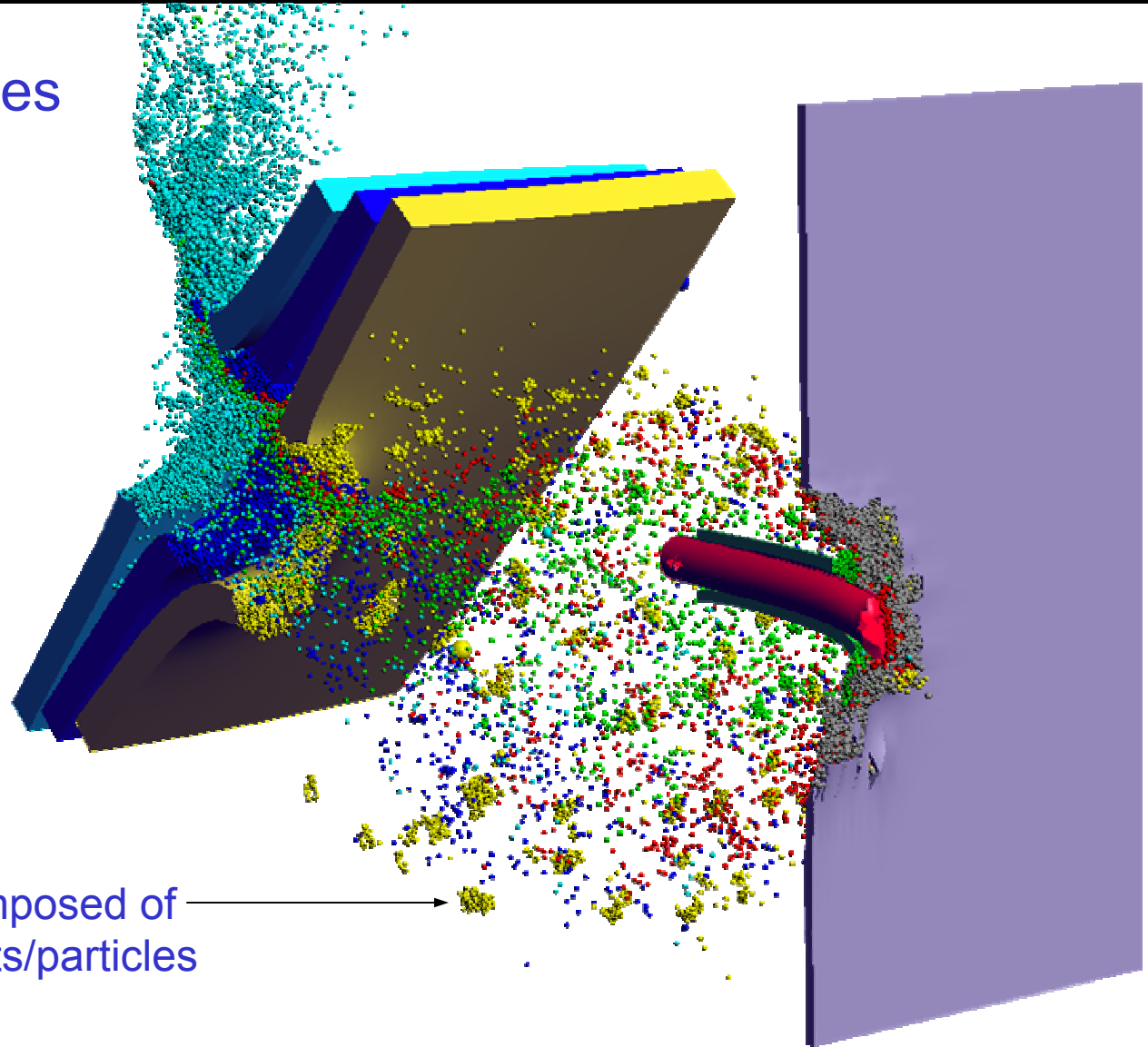


Conversion of finite elements to particles

Ballistic velocities

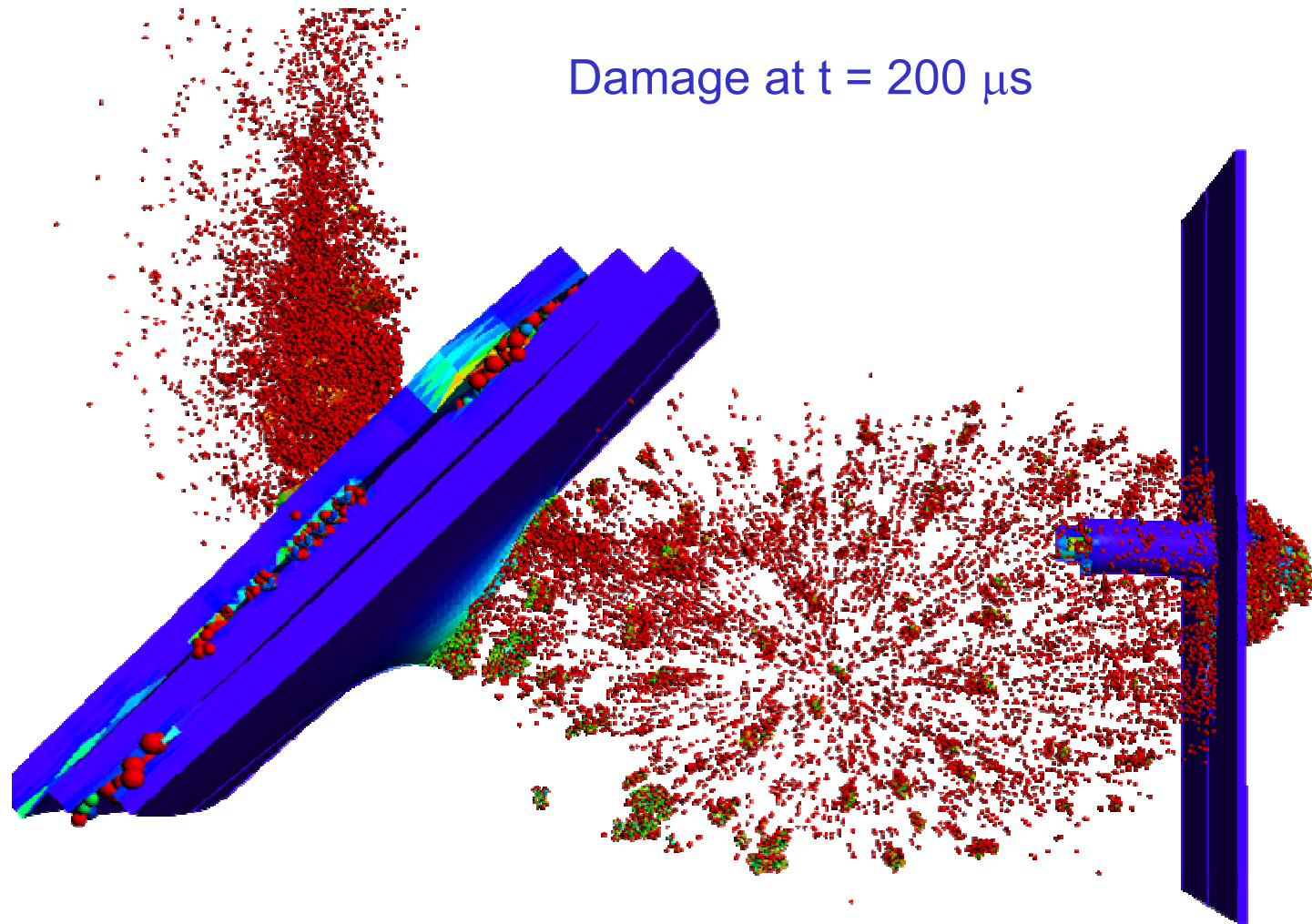
$V = 2000 \text{ m/s}$

$t = 200 \mu\text{s}$



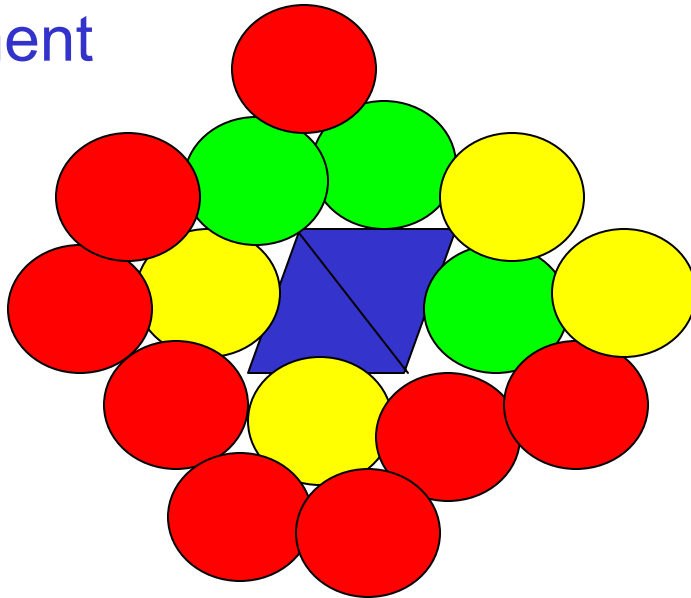
Fragments composed of multiple elements/particles

Conversion of finite elements to particles



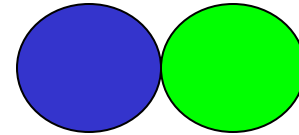
Description of computed fragments

Fragment

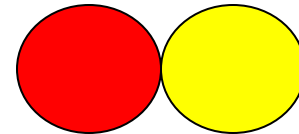


Red particles are failed ($D = 1.0$)

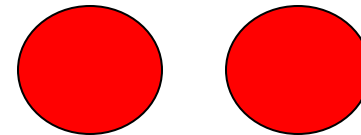
full bond



half bond



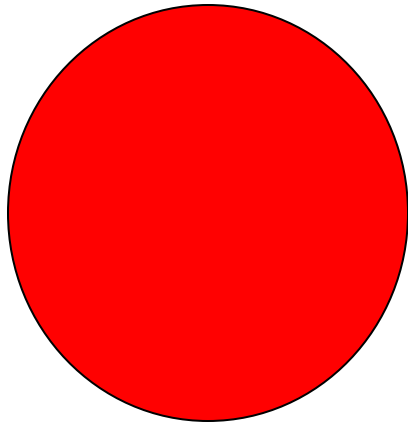
no bond



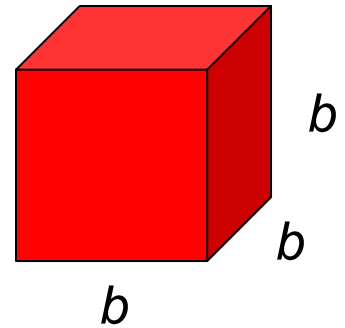
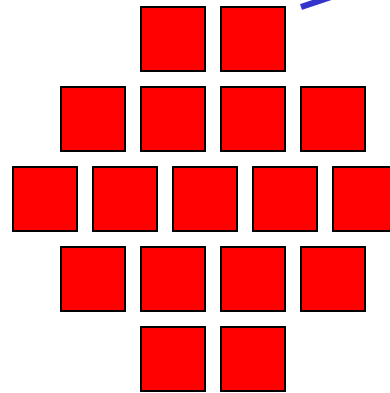
(compression only)

Estimate of small fragment sizes

It is possible to estimate the sizes of fragments smaller than the particles
(but probably not necessary)



Failed particle



From Grady

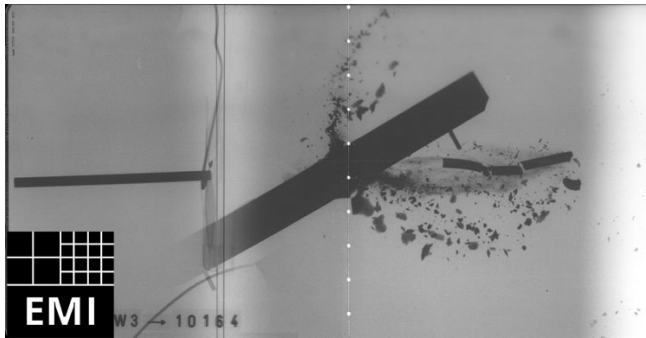
$$b = A \sqrt{\frac{\sigma}{\rho \dot{\epsilon}^2}}$$

Number of fragments per particle

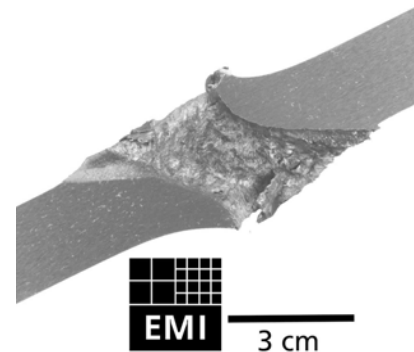
$$N = \text{Volume of particle} / b^3$$

Behind Armor Debris at ballistic velocities

N. Heider, K. Weber and P. Weidemaier, "Experimental and numerical simulation analysis of the impact process of structured KE penetrators onto semi-infinite and oblique plate targets," presented at 21st International Ballistics Symposium, 2004.



Radiograph during test



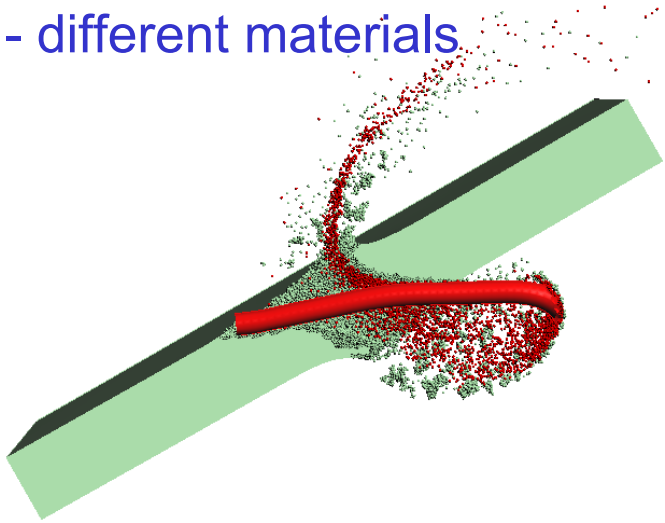
Section of recovered plate

- Tungsten rod ($L/D = 20$) impacting steel plate
- Impact velocity = 1615 m/s
- Impact obliquity = 60 degrees
- Angle of attack = 2.4 degrees (nose up)

Computed results at ballistic velocities

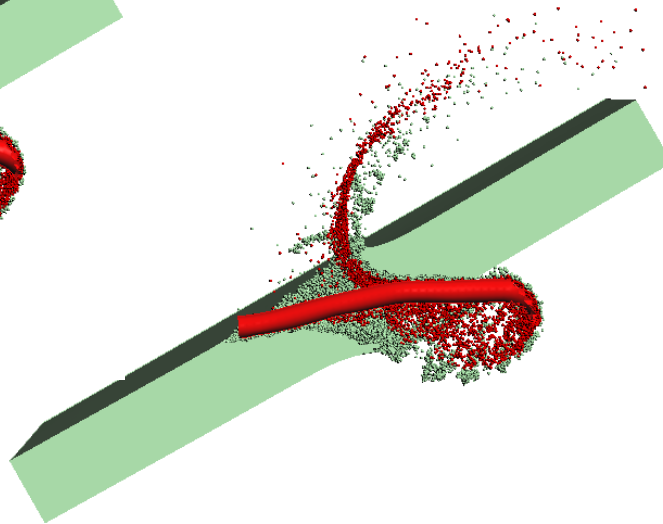
Baseline ($V = 1615$ m/s)

- impact conditions from test
- different materials

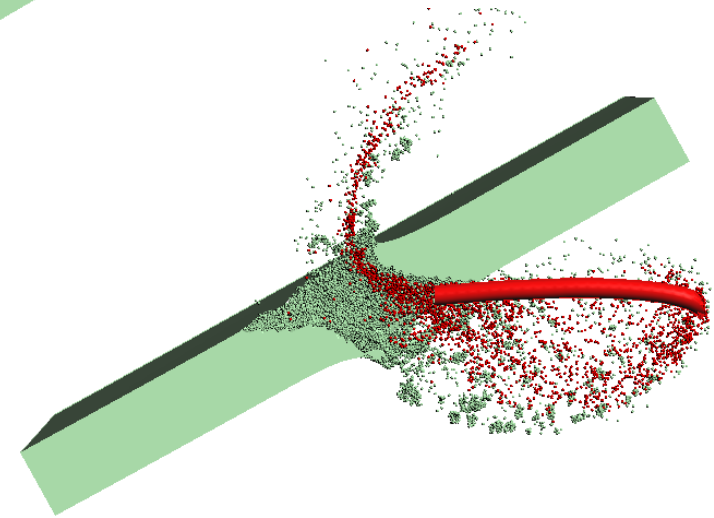


Computed responses at $80 \mu\text{s}$

- ### High-strength target
- 50 % stronger



- ### Constant kinetic energy
- higher velocity (25%)
 - lower mass

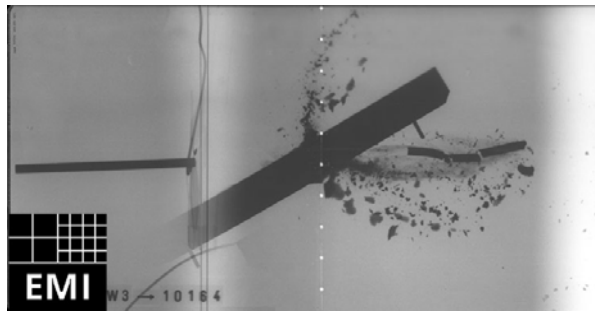


Computational and experimental results

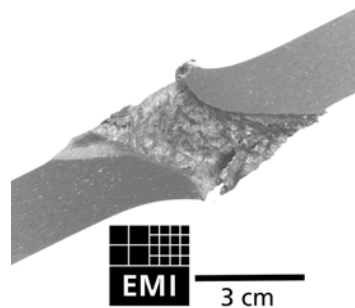
Computed damage at 168 μ s

Baseline

- impact conditions from test
- different materials



High-strength target



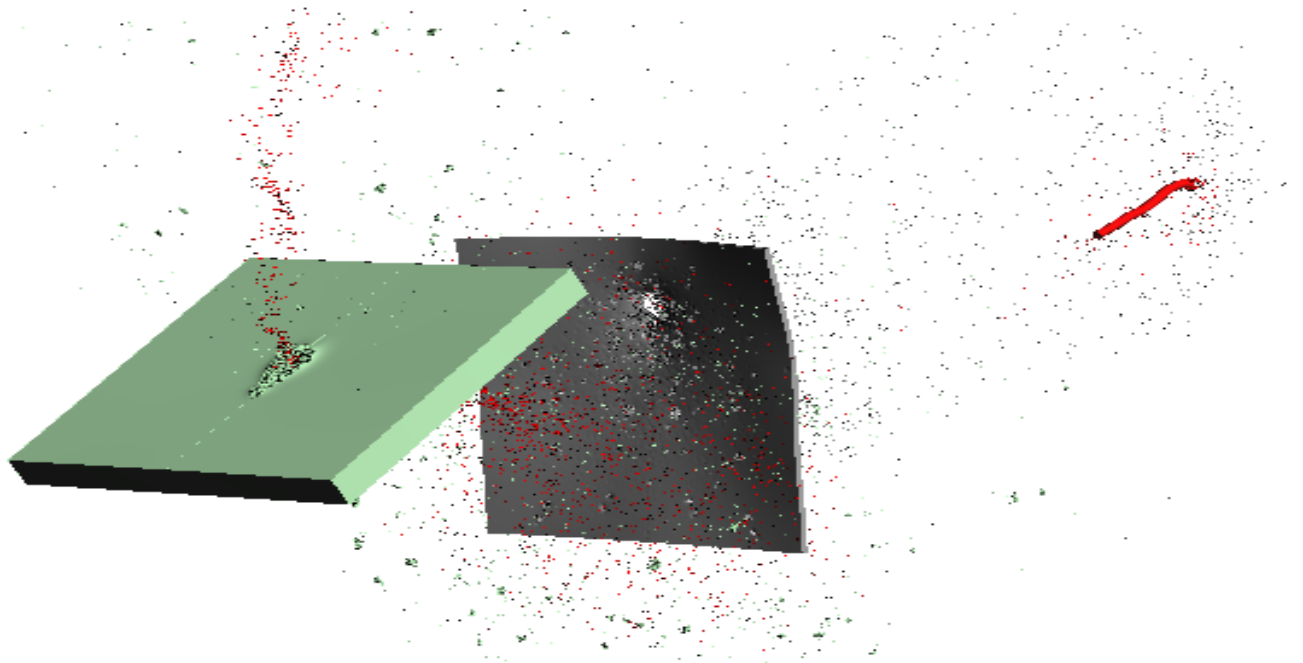
Constant kinetic energy

- higher velocity (25%)
- lower mass

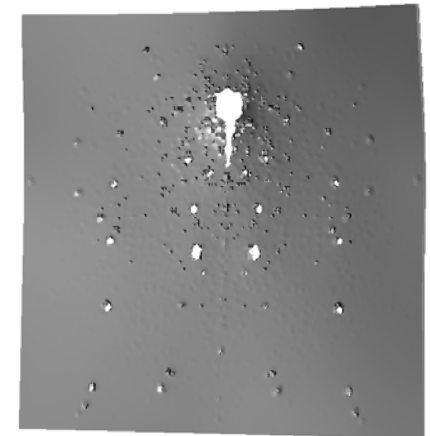


Baseline computation with witness plate

Computed response at 500 μ s

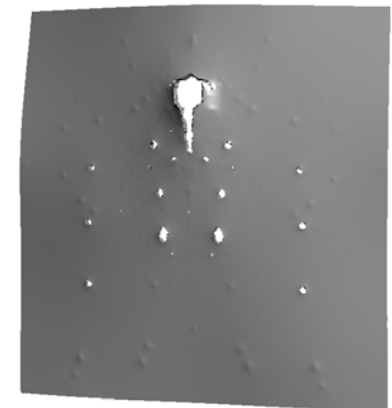


witness plate



front

back



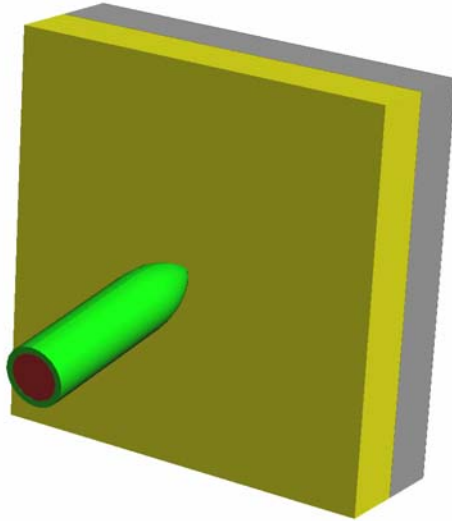
Thin aluminum witness plate placed behind target

- projectile and target fragments damage witness plate
- used to quantify behind armor debris

Layered ceramic/aluminum target

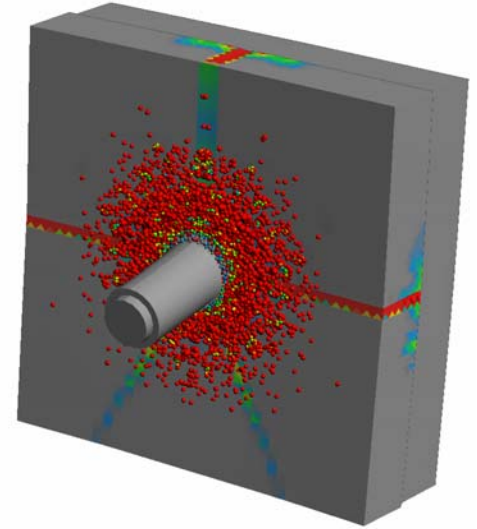
Projectile

- steel core
- copper jacket
- $V = 900$ m/s
- $\text{Ø} = 10$ deg

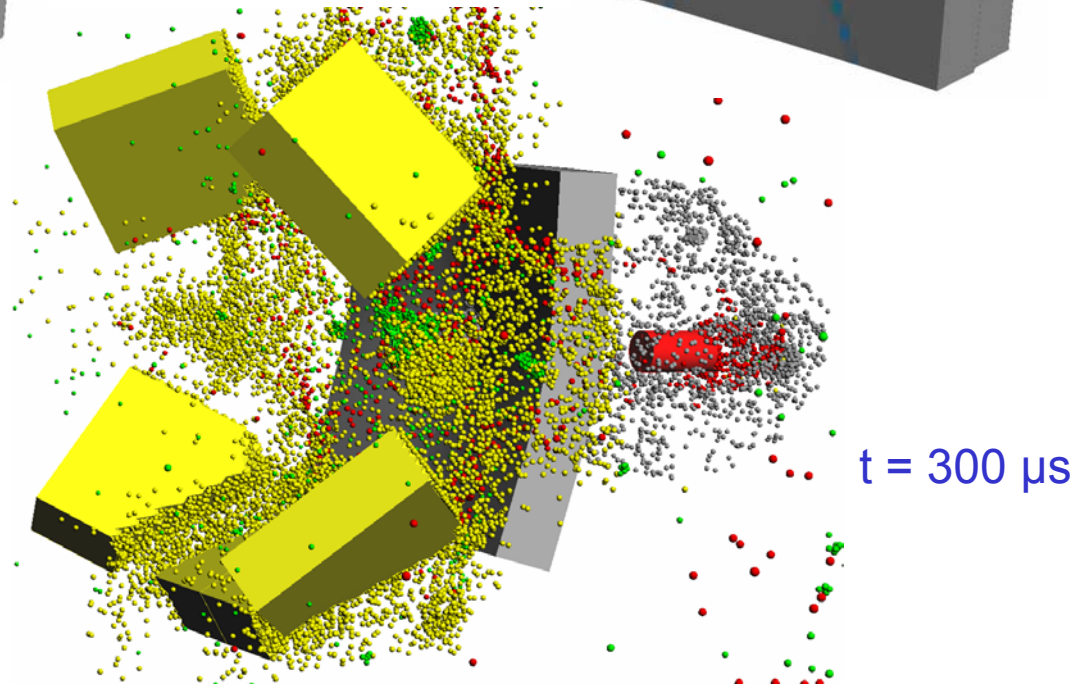
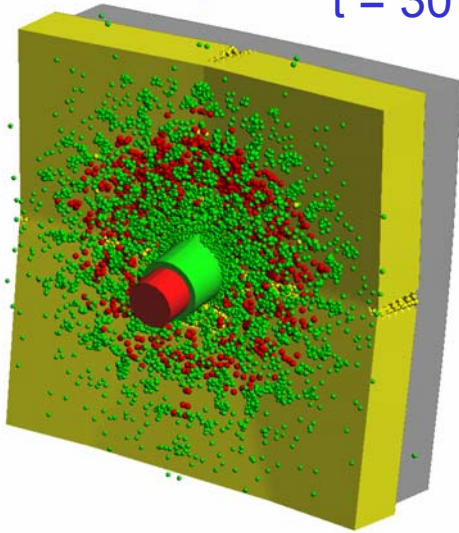


Damage

- $t = 20$ μs
- cracks form \longrightarrow
before conversion



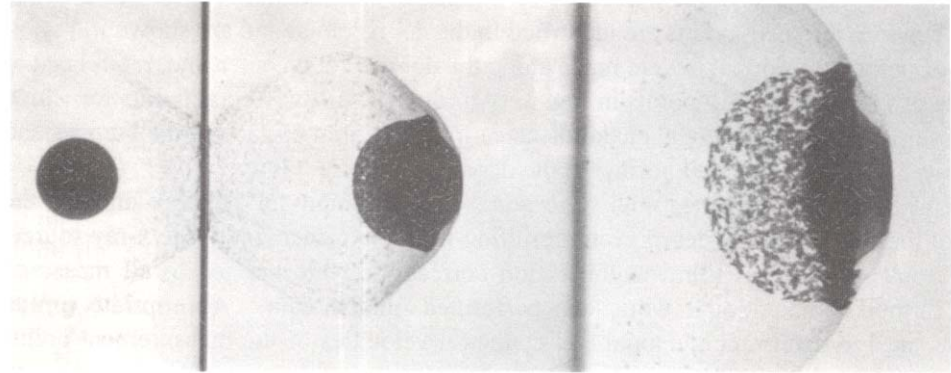
$t = 30$ μs



Computations of hypervelocity impact

Aluminum sphere impacting thin aluminum plate at 6.15 km/s

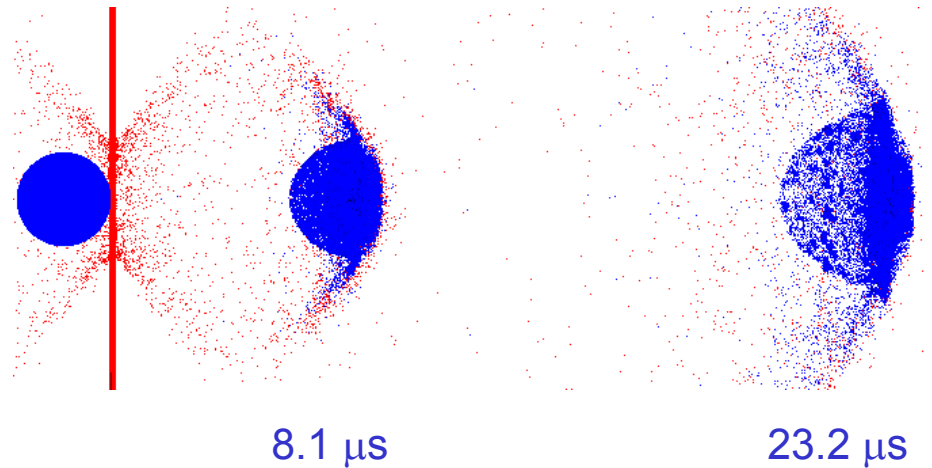
A. Piekutowski, "Effects of scale on debris cloud properties." Int. J. Impact Engng **20** (1997).



Computation using conversion:

- Shows same debris-cloud characteristics
- Position/scale of radiographs distorted by x-ray projection

Beissel, Gerlach, Johnson (HVIS 2005)



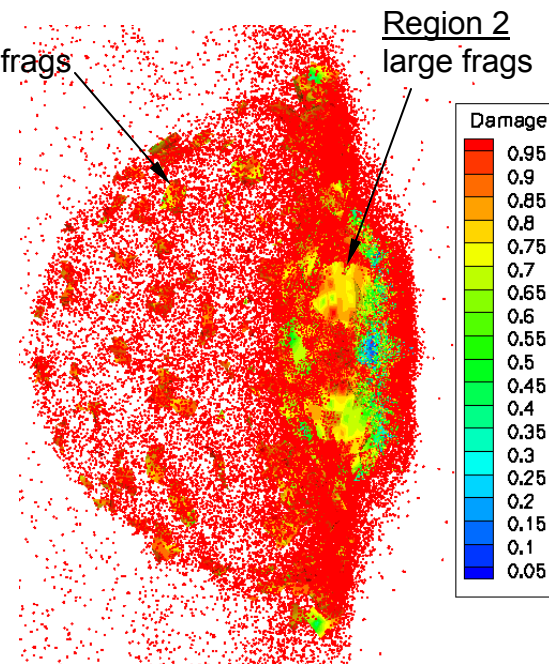
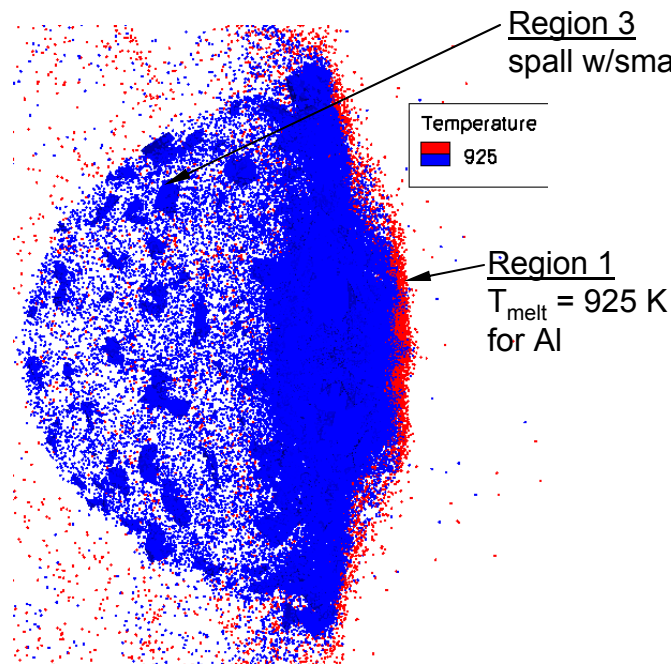
Computations of hypervelocity impact

Aluminum sphere impacting thin aluminum plate at 6.15 km/s

Three regions identified by Piekutowski in test:

1. Melted target and projectile at front
2. Large projectile fragments in middle
3. Small projectile fragments in spall

Temperature
at 23.2 μ s

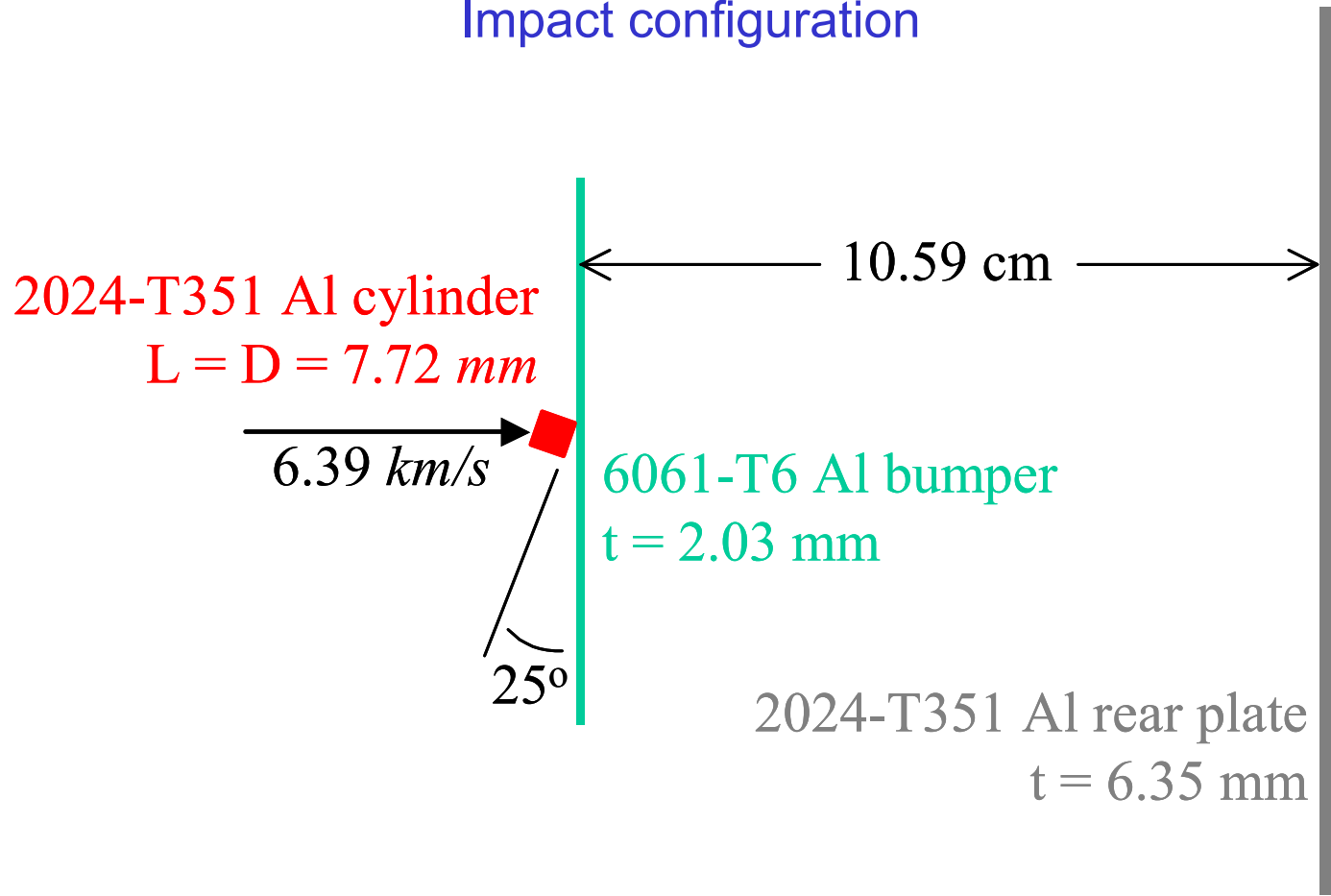


Damage
at 23.2 μ s

Computations of hypervelocity impact

Oblique cylinder impacting a Whipple shield

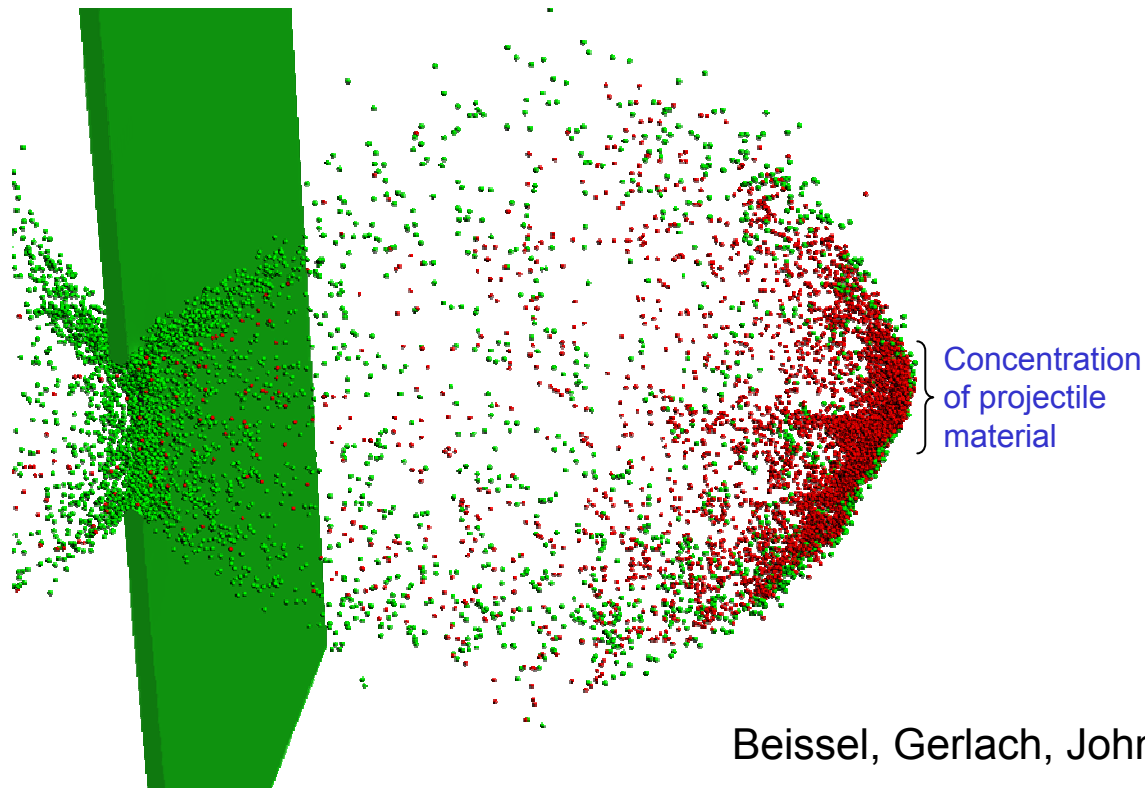
Impact configuration



Computations of hypervelocity impact

Oblique cylinder impacting a Whipple shield

Computed cross-section 15 μs after impact
(before debris cloud has reached rear plate)

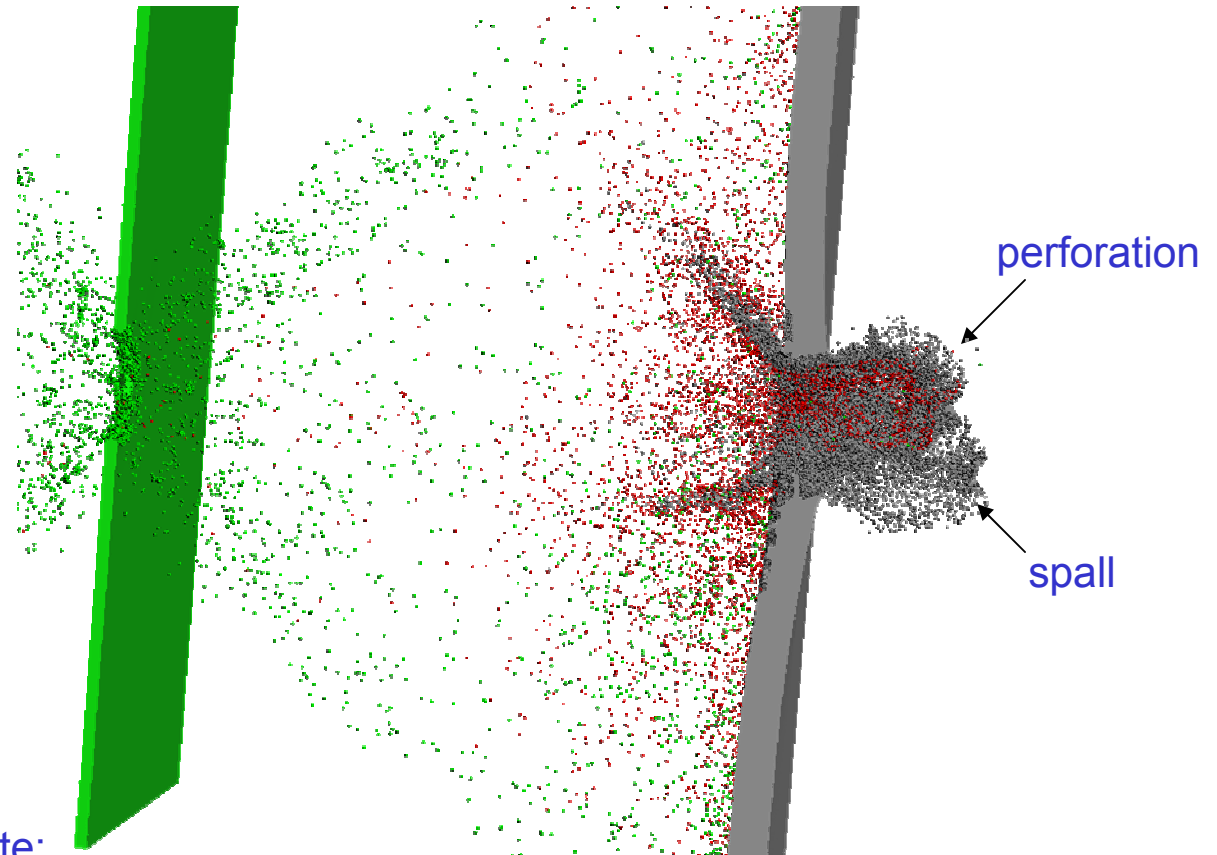


Beissel, Gerlach, Johnson (HVIS 2005)

Computations of hypervelocity impact

Oblique cylinder impacting a Whipple shield

Computed cross-section
50 μ s after impact



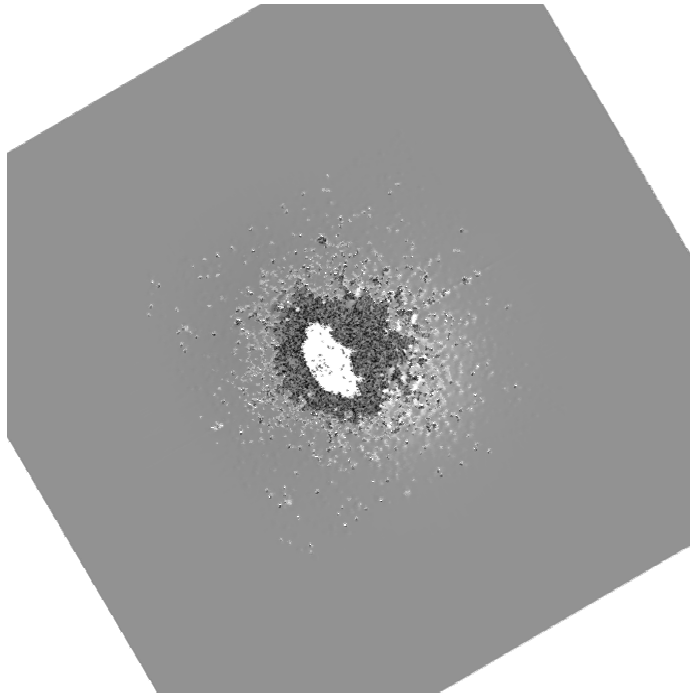
Two modes of failure in rear plate:

1. Perforation due to impact by concentration of projectile material in primary debris cloud
2. Spall due to impact by remaining projectile material in primary debris cloud

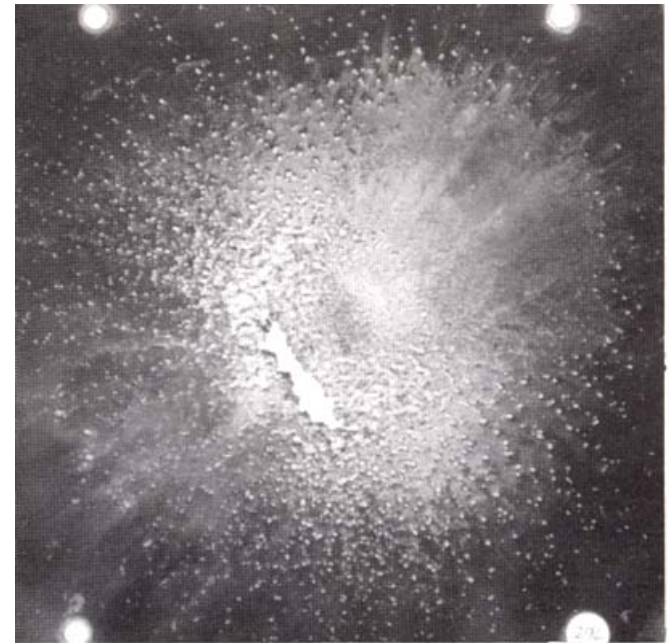
Computations of hypervelocity impact

Oblique cylinder impacting a Whipple shield

Computed rear plate 50 μ s after impact



A. Piekutowski, "Debris clouds generated by hypervelocity impact of cylindrical projectiles with thin aluminum plates." *Int. J. Impact Engng* **5** (1987).



Summary

- Combination of elements and particles is well suited for BAD computations
- Conversion algorithm enhances accuracy and efficiency of computations
- Demonstrated capability to compute BAD
 - includes travel through large air gaps
 - includes interaction with subsequent target plates/structures
- Demonstrated general agreement with test data

Behind Armor Debris movie

